PHYSICAL REVIEW C VOLUME 32, NUMBER 4 OCTOBER 1985

Elastic photon scattering from carbon and calcium and its interpretation

D. H. Wright,* P. T. Debevec, and L. J. Morford
Nuclear Physics Laboratory and Department of Physics, University of Illinois at Urbana-Champaign, Champaign, Illinois 61820

A. M. Nathan
University of Illinois at Urbana-Champaign, Champaign, Illinois 61820
and Département de Physique Nucléaire/MF, Centre d'Etudes Nucléaires de Saclay,
91191 Gif-sur-Yvette Cedex, France
(Received 12 February 1985)

Differential cross sections for the elastic scattering of tagged, monochromatic photons have been measured for targets of carbon and calcium between 19 and 52 MeV. The formalism for the interpretation of these cross sections in terms of the total photoabsorption cross section and its partitioning into $E1$ and $E2$ parts is presented. For carbon, we find excellent agreement between the photoabsorption deduced from the scattering and previous direct measurements. The fore-to-aft asymmetries in the cross sections indicate that the bulk of $E2$ strength is above 50 MeV and not between 30 and 45 MeV, as previously thought. For calcium, the scattering data indicate that the integrated photoabsorption cross sections per nucleon are closer to the nearly constant value reported for $A > 100$ than previously thought. No compact $E2$ strength exhausting more than 0.5 classical sums is found below 50 MeV, although weaker or less compact strength cannot be ruled out.

I. INTRODUCTION

The isovector giant quadrupole resonance (IVGQR) is a fundamental but largely unstudied normal mode of the nucleus. This is in contrast to the giant electric dipole resonance (GDR), which has been studied in exhaustive detail over the last 30 years, and the isoscalar giant quadrupole resonance (ISGQR), whose systematics have been well studied over the last 10 years. The GDR is so well studied in part because of the high dipole selectivity of the photon. As a consequence, most of what we know about the GDR has come from photon-induced reactions or their inverse. On the other hand, our knowledge of the ISGQR has come mainly from inelastic α scattering which, however, is ineffective in exciting the IVGQR. In fact, what little we know of the IVGQR has come mainly from photon-induced reactions, in which weakly excited $E2$ strength often gives rise to large observable effects through its interference with the dominant $E1$ strength. The signature of the $E1$-$E2$ interference is a fore-to-aft asymmetry in the angular distribution of the differential cross section. The technique of inferring $E2$ strength from these asymmetries has led to reports of $E2$ strength above the GDR, where the IVGQR is expected, in both (γ,p) (Ref. 1) and (γ,n) (Refs. 2 and 3) reactions (or their inverses). The latter of these has proven to be especially sensitive to resonant $E2$ strength because the nonresonant interaction that gives rise to fore-to-aft asymmetries is small. Such reactions are quite effective in determining the energy and width of the $E2$ strength distribution. However, extraction of the energy-weighted integrated strength, which can then be interpreted in terms of sum rules, requires the use of a model for the reaction, and is therefore somewhat more problematic.

Elastic photon scattering offers an alternate, seldom used method to study the systematics of the IVGQR. Although photon scattering is generally less sensitive than (γ,n) to $E2$ strength, it has the advantage that the interpretation of the data can be done in an essentially model-independent manner. This is due in part to the unique relationship between the elastic photon scattering cross section and the total photoabsorption cross section. A theoretical framework exists in which both the total photoabsorption cross section as well as the partitioning of this cross section into $E1$ and $E2$ parts can be deduced from the elastic scattering cross section. This framework has recently been used by the NBS (National Bureau of Standards) group on carbon and oxygen[4] and by the Mainz group on lead,[5] leading to reports of substantial $E2$ strength above the GDR in these nuclei.

In this paper, we report the measurement of photon scattering cross sections on carbon and calcium for incident photon energies between 19 and 52 MeV and the interpretation of these cross sections in terms of the distribution of $E1$ and $E2$ strength. A preliminary account of this work has been reported elsewhere.[6] The essential results of that report have not changed, and the present paper serves to provide both a detailed discussion of the experiment and its interpretation, and an improved formalism for that interpretation. In particular, we find no evidence for a large concentration of $E2$ strength in carbon between 30 and 45 MeV. Instead we find that the bulk of the $E2$ strength lies above 50 MeV. This directly contradicts the interpretation of the NBS scattering experiment by Dodge *et al.*,[4] who report about 2 classical sums of $E2$ strength in the 25—45 MeV range. We refer the reader to our previous publication for a discussion of the origin of that discrepancy.[6] We further find generally ex-

cellent agreement between the $E1$ photoabsorption inferred for carbon and the total photoabsorption cross section reported by Ahrens *et al.*[7] For calcium, a similar comparison reveals serious discrepancies with the measured photoabsorption cross section;[7] our results indicate a smaller photoabsorption cross section. The resulting integrated photoabsorption per nucleon is closer to the nearly constant value observed for medium and heavy nuclei.[8] The $E2$ situation in calcium is less clear than originally thought in that compact strength exhausting as much as 0.5 classical sums cannot be ruled out by the scattering data.

The remainder of this paper is organized as follows. The experimental technique is described in detail in Sec. II. The formalism which was used to interpret the scattering cross sections is presented in Sec. III, while a description of the actual interpretation is given in Sec. IV. Finally, a summary appears in Sec. V.

II. EXPERIMENTAL PROCEDURE

Elastic scattering cross sections on targets of carbon and calcium were measured using incident photon beams from the Illinois tagged photon facility and using a large-crystal NaI spectrometer to detect the scattered photon. The photon tagging process, depicted schematically in Fig. 1, is described as follows. An electron of a given energy undergoes bremsstrahlung in a thin foil, giving up some of its energy to the emitted photon. The post-bremsstrahlung electron is momentum analyzed and detected in the focal plane of a magnetic spectrometer. Energy conservation then requires that the balance of the original electron energy be carried off by the photon. Demanding a time coincidence between the detection of a scattered photon and the detection of a post-bremsstrahlung electron associates the photon with the electron and allows the photon energy to be deduced. The photon is thus "tagged" by an electron.

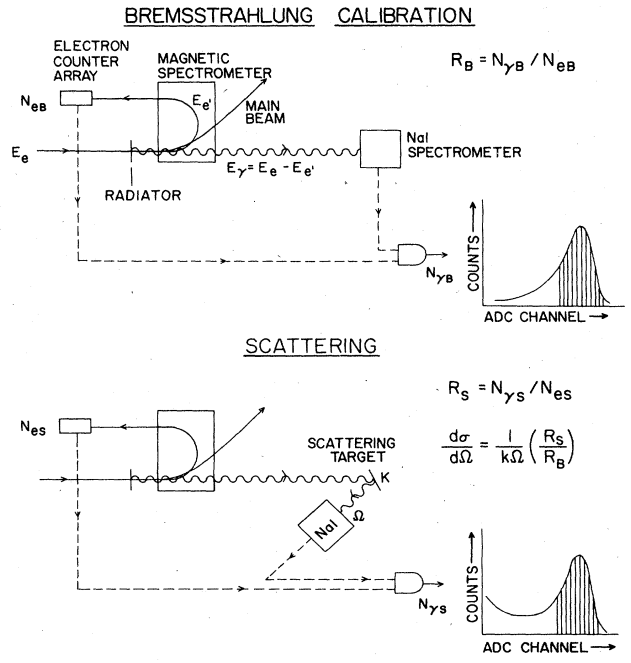

FIG. 1. Schematic drawing of the photon-scattering technique using tagged photons.

Electrons from the 100% duty factor accelerator MUSL-2 strike a 34.3 mg/cm^2 aluminum foil, with the result that about 0.3% of the electrons radiate a bremsstrahlung photon. Post-bremsstrahlung electrons are momentum analyzed in an inclined pole magnetic spectrometer and subsequently detected on the focal plane in a staircase array of 32 plastic scintillation counters, each subtending a momentum bite of approximately 1.25%. Under typical experimental conditions this corresponds to a 0.2 MeV wide energy bin. Data were taken with several beam energies, which allowed scattering cross sections to be measured with tagged photon energies ranging from 19 to 52 MeV.

Tagged photons are scattered from a cube of calcium 10.16 cm on a side or from a rectangular parallelepiped of graphite 10.16 cm thick with a face 15.24 cm square perpendicular to the beam. These targets have areal densities of 15.65 g/cm^2 and 15.75 g/cm^2, respectively.

Scattered photons are detected in a high efficiency, good resolution NaI spectrometer at angles of 135°, 90°, or 45°. The detector consists of a NaI(Tl) crystal, 25 cm in diameter and 30 cm long. It is gain-stabilized by an LED pulser which in turn is stabilized by a photodiode.[9] Surrounding the crystal is a 2.5-cm thick shield of $^6Li_2CO_3$, which serves as an effective absorber of slow neutrons. This in turn is nearly surrounded by an 11.4-cm thick annulus and disk of NE102 plastic scintillator which serves as an anticoincidence shield to reject events in which the electromagnetic shower is not fully contained in the NaI. It also is an effective moderator of neutrons. The entire NaI and anticoincidence combination is shielded from background radiation by at least 11.4 cm of lead. During these experiments the electron beam current was usually only a few nA. The resulting rate above 0.5 MeV in the NaI detector was between 10 and 200 kHz. At higher rates, the NaI pulses become distorted due to pileup. In order to avoid pileup and still have reasonably large photon rates above 20 MeV, a 29 g/cm^2 graphite absorber was placed in front of the NaI detector.

Data collection and experiment control were handled by an assembly language program on a PDP-15 computer, which was interfaced to the experiment through a combination of Illinois Black Box and CAMAC modules.

In a typical photon scattering experiment, the following procedure is used. First a calibration experiment is done in which the NaI is placed at 0°, as shown at the top of Fig. 1, directly into a photon beam of greatly reduced intensity. No target is placed in the beam. For each electron counter, the number of tagging electrons is counted for the duration of the calibration experiment, yielding N_{eB}. For each electron counter a pulse-height spectrum of photons in coincidence with these electrons is collected which represents the NaI response to monochromatic photons. A function which fits this spectrum is then integrated, for example, over the shaded region in Fig. 1, to

obtain the total number of tagged photons, $N_{\gamma B}$. The quantity of interest is $R_B = N_{\gamma B}/N_{eB}$, the so-called tagging efficiency, which is the number of detected tagged photons in the beam per tagging electron. For the scattering experiments a target is inserted into the photon beam and the NaI is placed at one of the scattering angles, as shown at the bottom of Fig. 1. Again, tagging electrons are counted for the duration of the scattering experiment to obtain N_{eS}, and a spectrum of scattered photons in coincidence with tagging electrons is collected. Integrating the function which fits this spectrum over the same region as for the calibration spectrum gives the total number of scattered, tagged photons, $N_{\gamma S}$. Again the relevant quantity is $R_S = N_{\gamma S}/N_{eS}$, which is the number of detected scattered tagged photons per tagging electron. The elastic scattering cross section, $d\sigma/d\Omega$, is given by

$$\frac{d\sigma}{d\Omega} = \frac{1}{k\Omega}\left[\frac{R_S}{R_B}\right], \tag{1}$$

where k is the number of target nuclei per unit area and Ω is the solid angle subtended by the detector. Note that this procedure is quite accurate because the same detector is used to detect scattered photons as is used to calibrate the incident flux. Since the response of the detector to monochromatic photons is measured, the absolute detector efficiency need never be determined. Sample pulse height spectra for an incident photon energy of 50 MeV are shown in Fig. 2. Several times during the experiment the NaI was rotated back to 0° for the collection of additional response spectra. This was done to ensure against relative changes in the normalization of the cross sections which may be caused by long term changes in beam parameters.

The technique for measuring electron-photon coincidences is described as follows. For each photon pulse above a threshold (usually set between 10 and 15 MeV), a 50 nsec wide pulse strobes 32 coincidence modules, one for each electron counter. Whenever an electron pulse arrives within the duration of the strobe, a signal is produced at the output which is synchronized with the electron pulse. The spectrum of time differences between this pulse and a pulse synchronized with the leading edge of the photon signal shows a peak near the center of the 50 nsec strobe, corresponding to true correlated events. Events falling within ±4.5 nsec of this peak are regarded as true coincidences. Other events are regarded as chance or accidental coincidences. For each of the 32 electron counters, the coincident photon signal is routed to one of four 256-channel arrays, depending on whether the coincidence was true or accidental and whether the photon energy was deposited entirely in the NaI ("accepted" event) or shared with the anticoincidence detector ("rejected" event).

The net coincidence spectrum is obtained by subtracting the appropriately scaled accidental spectrum from the coincidence spectrum. For scattering on calcium at 50 MeV and 45°, the ratio of true to accidental coincidences in the region of the photopeak is roughly 5 to 1.

The pulse height spectrum at 45° in Fig. 2 shows a steeply falling background in the energy region below the elastic scattering photopeak. This background is presumably due to atomic related events in the target, such as atomic Compton scattering and pair production followed by bremsstrahlung of the resulting particles. These events occur as true, correlated coincidences and produce a background which falls more or less exponentially with energy. No part of this background has been observed to extend beyond the energy of the elastic photopeak. It also is forward peaked and increases with the Z of the target. The spectrum of true nuclear events can be found by parametrizing the background and subtracting it from beneath the tail of the photopeak. Since the detailed energy dependence of the background is not known, this cannot always be done reliably, especially for very forward angles. However, at 45°, the atomic background beneath the photopeak was judged to be small enough that its subtraction does not introduce large uncertainties in the cross sections.

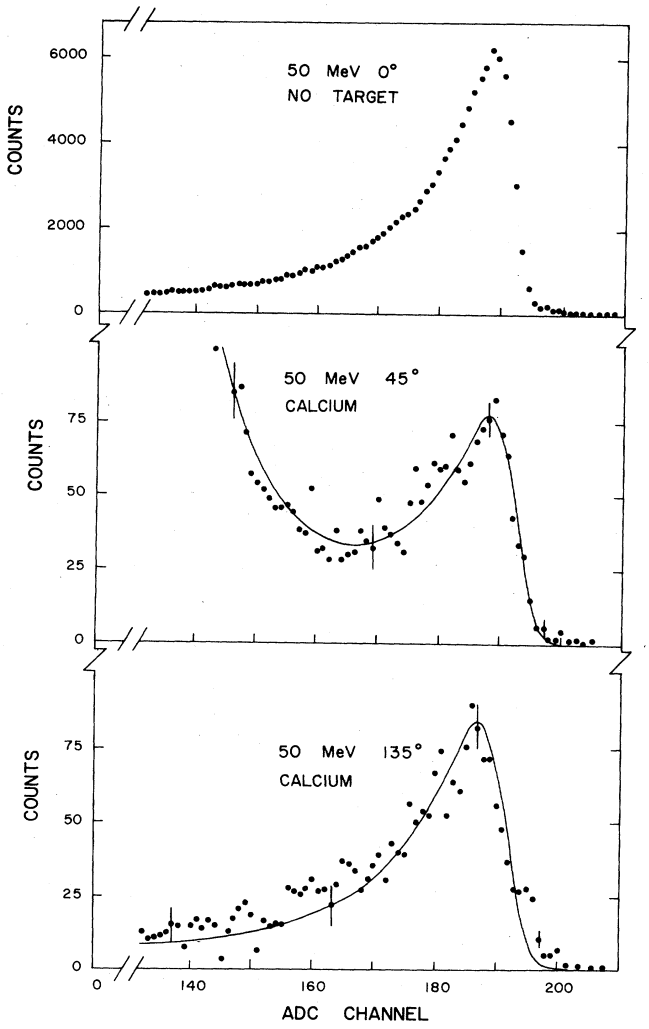

FIG. 2. Spectrum of incident (top) and scattered photons from a 50-MeV tagged photon beam.

The cross sections were obtained by fitting the spectra with a parametrized peak shape in the following manner. For both scattering and calibration experiments, spectra

from either four or eight contiguous electron counters were combined, each spectrum shifted slightly in energy so that their photopeaks coincide. This was done to improve the statistical precision of the data, at the cost of resolution in the photon energy. Since energy resolution was not an important criterion for the scattered photon spectrum, the "accepted" and "rejected" spectra were summed in order to determine the elastic cross sections. A parametrization of the photopeak in these experiments was determined by a least squares fit to the spectra. First a fit is performed to the response spectra obtained in the calibration experiment using a seven-parameter function consisting of the sum of a Gaussian peak and a low energy tail. The region of the fit extends from just above the ADC (analog-to-digital converter) threshold to just above the photopeak. This response function was then fitted to the scattering spectra at 135°. It was necessary to take into account the fact that the shape of the scattering spectrum is different from the corresponding response spectrum in that the amplitude of the tail relative to the amplitude of the photopeak was found to be consistently larger in the scattering spectrum than in the response spectrum. This is presumably due to the fact that in the scattering experiment the photons from the target diverge while in the calibration experiment the photons are in a nearly parallel beam. Therefore, in fitting to the scattering spectra, the amplitudes of the Gaussian and tail were allowed to independently vary, although the shapes of both of these were fixed to those shapes determined from the response function. The ratio R_S/R_B was determined by integrating the respective fitted functions. Despite the slightly different line shapes, this ratio was not very sensitive to the low-energy cutoff for the integration.

Once the parameters for the backward angle scattering

TABLE I. Elastic scattering cross sections for carbon.

	$d\sigma/d\Omega$ (μb/sr)		
E (MeV)[a]	$\theta=135°$	$\theta=90°$	$\theta=45°$
22.5	2.31(9)		2.32(14)
23.0	2.47(10)		2.58(14)
23.6	2.56(10)		2.67(14)
24.2	2.32(10)		2.35(14)
24.8	1.50(7)		1.45(10)
25.5	1.57(9)		1.72(13)
26.3	1.66(9)		1.68(12)
27.1	1.17(7)		1.15(10)
27.4	1.19(6)		1.16(6)
28.0	1.18(7)		1.27(7)
28.6	1.02(6)		1.13(7)
29.4	0.94(6)		0.92(5)
30.1	1.06(6)		1.20(6)
30.9	1.03(6)		1.13(6)
31.7	0.97(6)		1.12(6)
32.6	0.96(4)	0.63(4)	1.03(4)
33.4	0.91(4)	0.65(4)	0.98(5)
34.2	0.84(4)	0.60(4)	0.89(5)
35.1	0.86(5)	0.57(4)	0.86(5)
36.0	0.84(4)	0.59(4)	0.86(5)
36.9	0.82(4)	0.56(4)	0.89(4)
38.0	0.87(4)	0.54(3)	0.86(5)
39.1	0.84(4)	0.55(3)	0.94(4)
45.5	0.81(4)		0.78(4)
46.3	0.73(4)		0.82(4)
47.1	0.87(4)		0.84(4)
48.0	0.73(4)		0.77(4)
48.9	0.78(4)		0.87(4)
49.9	0.70(4)		0.80(4)
50.9	0.68(4)		0.86(5)
52.0	0.70(4)		0.86(4)

[a] The energy averaging interval for a given data point is the difference of the energies of the given point and the previous or following point.

function have been found, fitting the forward angle data at the same energy requires only that the overall amplitude and position of the peaks vary in the fit. It is assumed here that the shape of the scattering function is independent of scattering angle. All other parameters are identical to those of the backward angle fit and are held fixed. For these angles a parametrized function describing the atomic background is included in the fit.

The calculation of the cross section is completed with the determination of the factors k and Ω in Eq. (1). Because of the size of the targets, these quantities cannot be treated independently; their product was calculated by a multidimensional numerical integration, using information about the photon beam profile and including the attenuation of the photons in the target.

The resulting elastic cross sections are presented in Tables I and II. The uncertainties include statistical errors only. The systematic uncertainty in the cross section scale is estimated to be $\pm 5\%$. The present results for carbon are in excellent agreement with the NBS results. Inelastic scattering, when it occurred, was treated as a secondary photopeak. The inelastic cross sections for carbon are presented in Table III, and a sample spectrum showing inelastic scattering in carbon is shown in Fig. 3. No inelastic scattering was observed in calcium.

III. FORMALISM FOR THE INTERPRETATION OF THE ELASTIC CROSS SECTIONS

The basic goal of this analysis will be to use the elastic scattering cross section $d\sigma/d\Omega(E,\theta)$ to deduce useful information about the total photoabsorption cross section $\sigma_\gamma(E)$ and its multipole composition. This is possible because of the close link between $d\sigma/d\Omega$ and σ_γ. Although

TABLE II. Elastic scattering cross sections for calcium.

E (MeV)[a]	$d\sigma/d\Omega$ (μb/sr) $\theta=135°$	$\theta=90°$	$\theta=45°$
19.3	33.51(62)	21.91(55)	34.80(100)
20.0	37.99(69)	25.58(59)	38.22(93)
20.7	36.44(80)	24.78(69)	34.59(97)
21.4	31.90(69)	22.41(62)	31.52(83)
22.2	26.91(61)	18.35(50)	30.10(71)
23.0	21.69(54)	14.69(48)	25.36(66)
23.8	18.09(50)	12.57(44)	20.53(61)
24.8	16.13(43)	10.99(40)	18.67(50)
25.2	15.52(46)		17.31(67)
25.9	14.60(45)		17.53(62)
26.6	14.00(40)		15.97(52)
27.4	12.36(38)		15.89(48)
28.2	11.50(42)		14.78(48)
29.1	10.94(35)		13.67(36)
30.0	11.05(36)		14.24(36)
31.0	10.70(36)		13.45(34)
31.4	11.07(42)	7.56(25)	12.27(51)
32.3	10.96(45)	7.19(26)	12.13(52)
33.2	10.21(41)	7.18(24)	11.62(46)
34.2	9.91(43)	7.03(26)	11.43(45)
35.2	9.34(36)	6.66(21)	10.94(37)
36.3	9.01(39)	6.84(24)	10.16(38)
37.4	8.71(37)	6.67(22)	10.64(34)
38.8	7.86(27)	6.11(22)	10.12(27)
40.2	7.82(25)		9.46(41)
41.7	6.90(28)		9.56(38)
43.4	6.46(24)		9.52(39)
44.1	6.55(19)	5.23(19)	9.39(34)
45.8	6.16(17)	4.82(18)	8.57(29)
47.8	5.52(17)	4.98(17)	8.45(27)
50.0	5.39(16)	4.07(15)	7.77(25)

[a] The energy averaging interval for a given data point is the difference of the energies of the given point and the previous or following point.

TABLE III. Inelastic scattering cross sections at 135° on carbon, in which the target is left in the 4.44 MeV first excited state.

Energy interval (MeV)	$d\sigma/d\Omega$ (μb/sr)
22.3–23.2	0.35(3)
23.3–24.4	0.31(3)
24.6–25.8	0.23(3)
26.0–27.3	0.16(3)
27.1–28.2	0.21(3)
28.4–29.6	0.23(3)
29.8–31.2	0.22(3)
31.4–32.9	0.14(2)
45.1–46.7	0.12(3)
46.7–48.5	0.15(3)
48.5–50.4	0.14(3)

the formalism necessary to establish this link has been presented elsewhere,[4,5] we find it convenient to summarize the relevant features here.

We start by writing the elastic cross section as the square of the modulus of a complex scattering amplitude:

$$\frac{d\sigma}{d\Omega}(E,\theta)=|R(E,\theta)|^2 . \tag{2}$$

In the forward direction ($\theta=0°$), $R(E,0°)$ is uniquely related to $\sigma_\gamma(E)$. We first write

$$R(E,0°)=f(E)+D_0 , \tag{3}$$

where $f(E)$ is the complex forward amplitude for scattering from the internal degrees of freedom of the nucleus, and D_0 is the classical Thomson amplitude for the scattering of photons from a point object of charge Ze and mass AM:

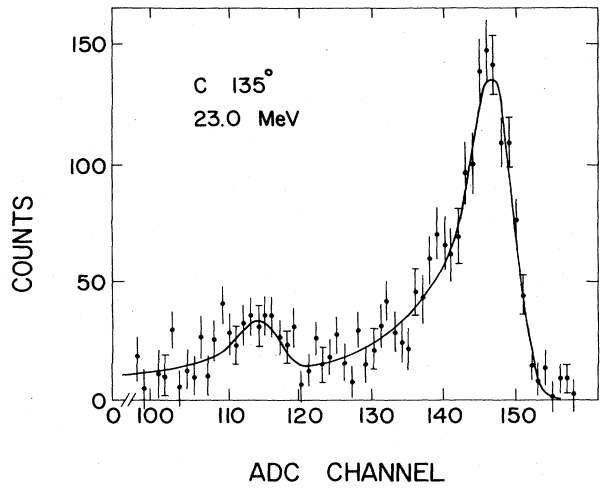

FIG. 3. Spectrum of scattered photons from carbon. The peak in channel 146 is due to elastic scattering, and the peak in channel 114 is due to inelastic scattering, leaving the nucleus in the 4.44-MeV first excited state.

$$D_0=\frac{-(Ze)^2}{AMc^2}\equiv-\frac{Z^2}{A}r_0 , \tag{4}$$

where $r_0=e^2/Mc^2$ is the classical radius of the proton. Other possible contributions to the coherent scattering amplitude (e.g., atomic Rayleigh and Delbrück) are small at the energies and scattering angles of interest here and will not be considered further. A low-energy theorem states that in the limit of zero energy, the total scattering amplitude is just D_0. On the other hand, $f(E)$ is linked to $\sigma_\gamma(E)$ through the optical theorem

$$\mathrm{Im}[f(E)]=\frac{E}{4\pi\hbar c}\sigma_\gamma(E) , \tag{5}$$

and a dispersion relation

$$\mathrm{Re}[f(E)]=\frac{E^2}{2\pi^2\hbar c}\mathrm{P}\int_0^\infty\frac{\sigma_\gamma(E')}{E'^2-E^2}dE' , \tag{6}$$

where P denotes the principal value of the integral. Equations (3)—(6) imply that $\sigma_\gamma(E)$ uniquely specifies the forward elastic cross section $d\sigma/d\Omega(E,\theta=0°)$.

Before proceeding further, it is useful to recall the fundamental physics upon which Eqs. (4)—(6) are based. The low-energy theorem that gives rise to Eq. (4), the Thomson limit, effectively states that at very low energies the scattering amplitude is determined by the total charge and total mass, regardless of the composition of the system.[10,11] This is both physically appealing and theoretically sound, as it is based on gauge invariance. It has been verified experimentally many times. The optical theorem, Eq. (5), is equally sound, as it is based on the principle of unitarity. The forward dispersion relation (DR), Eq. (6), is somewhat more difficult to characterize. Although this is a model-independent relationship, based on a sound physical principle (microcausality),[12] it has been pointed out several times in the literature that one must be very careful applying the DR in the context of any particular model.[13] For example, the use of the DR in a nonrelativistic model leads to contradictions. This could be easily predicted, since a nonrelativistic model violates microcausality. Furthermore, in applications where one uses experimentally measured values for $\sigma_\gamma(E)$ to numerically compute the DR, practical difficulties arise due to the extension of the principal value integral to infinity, although this difficulty is somewhat mitigated by the energy weighting in the denominator of the integrand. In the analysis to follow, we will terminate the dispersion integral at the pion mass $m_\pi c^2$. The neglected contribution, which is due essentially to subnucleon degrees of freedom, will be absorbed into the Thomson amplitude, thereby introducing an effective energy dependence to that amplitude.[14] This will be discussed more fully below.

The preceding discussion means that one can uniquely predict the forward elastic scattering cross section if one knows $\sigma_\gamma(E)$ everywhere. In order to predict the scattering at arbitrary θ, one needs additional information. First, part of the scattering amplitude [$f(E)$ in the forward direction] is due to the real or virtual excitation of intermediate states of definite spin and parity. These spins and parities, or equivalently the multipole composition of $\sigma_\gamma(E)$, will determine, in part, the angular distribu-

tion of the scattered photon. In order to proceed, we first decompose $\sigma_\gamma(E)$ and $f(E)$ into multipoles:

$$\sigma_\gamma(E)=\sum_\lambda \sigma_\gamma^\lambda(E) ,$$
$$f(E)=\sum_\lambda f^\lambda(E) , \tag{7}$$
$$\lambda = E1, M1, E2, \ldots .$$

Then one can show that in the long wavelength limit, where the only relevant multipoles are $E1$, $M1$, and $E2$, the optical theorem and dispersion relation hold for *each multipole separately*:[15,16]

$$\mathrm{Im}[f^\lambda(E)]=\frac{E}{4\pi\hbar c}\sigma_\gamma^\lambda(E) ,$$
$$\mathrm{Re}[f^\lambda(E)]=\frac{E^2}{2\pi^2\hbar c}\int_0^{m_\pi c^2}\frac{\sigma_\gamma^\lambda(E')}{E'^2-E^2}dE' . \tag{8}$$

As discussed above, the integral is terminated at $m_\pi c^2$. The scattering amplitude assumes the form

$$R(E,\theta)=\sum_\lambda f^\lambda(E)g_\lambda(\theta)+D(E,\theta) , \tag{9}$$

where the $g_\lambda(\theta)$ are the angular factors appropriate to each multipole, with the normalization $g_\lambda(0)=1$. The $g_\lambda(0)$ are given in Table IV. In this expression, we have anticipated the result that at finite energy and scattering angle, the amplitude $D(E,\theta)$ differs from the low energy Thomson limit given by Eq. (4). This modification arises because part of the Thomson amplitude is the coherent superposition of amplitudes of waves scattered from the fundamental scattering centers in the nucleus. These centers may be the nucleons themselves (especially the protons) or, in the presence of exchange forces, the charged mesons that are exchanged between pairs of nucleons. This term must be modified at finite momentum transfer $q=(2E/\hbar c)\sin(\theta/2)$ by one or more form factors in order to properly account for the phase relation among waves scattered from different points in the nuclear volume. The finite size of the nucleus, therefore, introduces a q dependence to the Thomson amplitude. This modification has been previously discussed.[4,5,17] In addition, the fact that we terminate our dispersion integral at $m_\pi c^2$ introduces an energy dependence to this same part of the Thomson amplitude. This is the result of the nonlocality due to the finite size of the scattering centers themselves.[14] For example, the effect of the excited states of the nucleon (e.g., the delta), which have been eliminated from the dispersion integral, show up instead in the Thomson amplitude. Similar reasoning leads one to expect an energy dependence to the exchange scattering, since these processes are inherently nonlocal.[18] The expression that we use for the modified Thomson amplitude is

$$D(E,\theta)=\left[-Zr_0F_1(q)h_1(E,\theta)-\frac{NZ}{A}\kappa r_0F_2(q)h_2(E,\theta)+\frac{NZ}{A}r_0(1+\kappa)\right]g_{E1}(\theta) , \tag{10}$$

where κ is the enhancement to the classical sum rule for the unretarded dipole operator:

$$\int\sigma_\gamma^{\mathrm{unret},E1}(E)dE=2\pi^2\frac{NZ}{A}r_0(1+\kappa) . \tag{11}$$

The form factors $F_i(q)$ and the nonlocality corrections $h_i(E,\theta)$ are normalized to be unity at $E=0$, so that

$$\lim_{E\to0}D(E,\theta)=-\frac{Z^2}{A}r_0\,g_{E1}(\theta)=D_0\,g_{E1}(\theta) , \tag{12}$$

as required by the low energy theorem.

For the scattering from nucleons [the first term in Eq. (10)], the form factor $F_1(q)$ is the same quantity that is measured in elastic electron scattering and is well known for both C and Ca.[19] The nonlocality correction factor $h_1(E,\theta)$ has been discussed by Drechsel and Russo.[20] They find

$$-Zr_0F_1(q)h_1(E,\theta)g_{E1}(\theta)$$
$$=-ZF_1(q)\left\{\left[r_0-\bar\alpha\left[\frac{E}{\hbar c}\right]^2\right]g_{E1}(\theta)-\bar\beta\left[\frac{E}{\hbar c}\right]^2g_{M1}(\theta)\right\} , \tag{13}$$

where

$$\bar\alpha=\alpha_R+\frac{A}{Z}\alpha_E$$

and

$$\bar\beta=\frac{A}{Z}\beta_p+\left[\frac{5}{6}\frac{A}{Z}+\frac{1}{6}\right]\beta_D . \tag{14}$$

In these expressions, α_E is the electric polarizability of the nucleon, α_R is a recoil correction, and β_p and β_D are the paramagnetic and diamagnetic susceptibilities, respectively, of the nucleon. Drechsel and Russo[20] estimate these quantities in a nonrelativistic constituent quark model:

$$\alpha_E=12.2\times10^{-4}\ \mathrm{fm}^3 ,$$
$$\alpha_R=1.5\times10^{-4}\ \mathrm{fm}^3 ,$$
$$\beta_p=7.5\times10^{-4}\ \mathrm{fm}^3 , \tag{15}$$
$$\beta_D=-6.0\times10^{-4}\ \mathrm{fm}^3 .$$

They also emphasize that their treatment is only approximate in that it does not include possible corrections to these quantities when a nucleon is imbedded in the nuclear medium.

TABLE IV. Angular factors for the elastic scattering amplitude. $(\hat{\mathbf{k}},\hat{\boldsymbol{\epsilon}})$ is the incident direction and polarization and $(\hat{\mathbf{k}}',\hat{\boldsymbol{\epsilon}}')$ is the scattered direction and polarization. λ labels the multipolarity.

λ	$g_\lambda(\theta)$
$E1$	$\hat{\boldsymbol{\epsilon}}\cdot\hat{\boldsymbol{\epsilon}}'$
$M1$	$(\hat{\boldsymbol{\epsilon}}\times\hat{\mathbf{k}})\cdot(\hat{\boldsymbol{\epsilon}}'\times\hat{\mathbf{k}}')$
$E2$	$(\hat{\boldsymbol{\epsilon}}\cdot\hat{\boldsymbol{\epsilon}}')(\hat{\mathbf{k}}\cdot\hat{\mathbf{k}}')+(\hat{\boldsymbol{\epsilon}}\cdot\hat{\mathbf{k}}')(\hat{\boldsymbol{\epsilon}}'\cdot\hat{\mathbf{k}})$

On the other hand, the parameters associated with the exchange scattering [the second term in Eq. (10)] are less well known. The parameter κ can be determined if one knows $\sigma_\gamma^\lambda(E)$. However, the exchange form factor is poorly known. Arenhövel[21] has suggested that a reasonable first approximation might be

$$F_2(q)=[F_1(q/2)]^2 , \tag{16}$$

corresponding to scattering from a completely uncorrelated pair of nucleons. A better approximation can be achieved by introducing correlations at short distances. In the analysis to follow, we will try various assumptions for $F_2(q)$ and show that, since the present data involve low q, the conclusions we draw are not too sensitive to the exact form of $F_2(q)$. Similarly, the nonlocality correction $h_2(E,\theta)$ associated with the exchange scattering is not well known. General considerations suggest that since the range of the nonlocality should be on the order of $h/m_\pi c$, then the corresponding scattering amplitude should not vary appreciably with E as long as $E \ll m_\pi c^2$. Explicit calculations for the special case of the deuteron support this intuition.[18,22] In the analysis to follow, we simply assume no energy dependence, i.e., $h_2(E,\theta)=1$.

To summarize, we will use Eq. (9) to predict the elastic scattering amplitude at any energy and angle. The cross section is found by averaging the square of the modulus of this amplitude over the two polarization states of the incident photon and summing over the two states of the outgoing photon. This will require both the "resonance" amplitudes $f^\lambda(E)$ and the modified Thomson amplitude $D(E,\theta)$. Assumptions will be made about the $\sigma_\gamma^\lambda(E)$, which are used to calculate the $f^\lambda(E)$ via Eq. (8). Since the long wavelength limit should be applicable to C and Ca below 50 MeV, the multipoles are restricted to $E1$, $M1$, and $E2$. The modified Thomson amplitude is calculated from Eq. (10). The parameter κ is calculated from the $\sigma_\gamma^\lambda(E)$. For the scattering from nucleons, the experimentally determined charge form factor $F_1(q)$ (see Table V) and the prescription of Drechsel and Russo are used. For the exchange scattering, the suggestion of Arenhövel [Eq. (16)] is used for the form factor and the amplitude is assumed to be energy independent. For those corrections that are model dependent, we will test the sensitivity of our results to that model.

IV. INTERPRETATION OF THE ELASTIC CROSS SECTIONS

A. General considerations for the analysis

It will be the goal of the analysis to use the scattering data themselves in order to determine the $\sigma_\gamma^\lambda(E)$. These can then be interpreted in terms of giant resonances, sum rules, widths, etc. The formalism described in Sec. III implies that if one knows the $\sigma_\gamma^\lambda(E)$, one can predict the scattering cross section in an essentially model independent way. In general, it is not possible to reverse the process, namely to uniquely determine the $\sigma_\gamma^\lambda(E)$ from $d\sigma/d\Omega(E,\theta)$. The reason is quite clear. The $\sigma_\gamma^\lambda(E)$ are directly related to the imaginary part of the scattering amplitude, whereas the scattering cross section involves an incoherent sum of both real and imaginary parts. The phase of the scattering amplitude is lost so that a separation into real and imaginary parts is not possible. However, the real and imaginary parts are not independent but are related by the DR. Recall that the DR relates the real amplitude at a given energy to an integral of the imaginary part over all energies. Thus it seems reasonable that if one has measured $d\sigma/d\Omega(E,\theta)$ over the full energy range for which the $\sigma_\gamma^\lambda(E)$ are important, it should be possible to extract the $\sigma_\gamma^\lambda(E)$ from these data. Moreover, in many cases it is not necessary to have scattering data beyond about 50 MeV in order to determine the $\sigma_\gamma^\lambda(E)$ below 50 MeV. The reason is that for most, if not all, nuclei, the behavior of $\sigma_\gamma(E)$ in the so-called quasi-deuteron (QD) region between 40 MeV and $m_\pi c^2$ is a well-known universal function that scales with NZ/A.[8] Therefore, if one constrains $\sigma_\gamma(E)$ above 40 MeV to be this universal function, the scattering data up to 50 MeV can be used to extract the $\sigma_\gamma^\lambda(E)$ below about 40 MeV. Since this is just the region where giant resonances are expected, we can expect elastic photon scattering to be a useful tool for studying the location, width, integrated strength, etc., of the low multipole giant resonances (mainly $E1$ and $E2$).

Having established that it should be possible, in principle, to extract the σ_γ^λ from $d\sigma/d\Omega(E,\theta)$, we must face the problem of determining three independent functions σ_γ^{E1}, σ_γ^{M1}, and σ_γ^{E2}. For both C and Ca, σ_γ^{M1} is expected to be contained in isolated, bound levels whose properties are already known. Therefore, we need only extract two independent functions, σ_γ^{E1} and σ_γ^{E2}, from the scattering data. We have developed a technique for decoupling the extraction of these two functions. The key is to recognize that the $E2$ contribution to the scattering cross section occurs primarily through the interference with the $E1$, which dominates at all energies. This interference results in an angular distribution which is antisymmetric about 90° ($\alpha\cos^3\theta$).[4] Thus if one constructs scattering data that have been averaged over angles symmetric about 90°, the resulting data should be sensitive mainly to σ_γ^{E1}. One therefore analyzes these angle-averaged data to obtain a first estimate for σ_γ^{E1}, essentially independent of any $E2$ strength that might be present. This estimate can then be used as a starting point for a second iteration, in which the full unaveraged data are analyzed in order to obtain an improved σ_γ^{E1} as well as to determine σ_γ^{E2}. In particular, the fore-to-aft asymmetries should be indicative of the presence of $E2$ strength. In this regard, it is worth noting that, unlike the (γ,n) reaction, one expects nonresonant asymmetries due to the various form factors. Furthermore, an asymmetry measured at a given energy in (γ,n) necessarily means that there is $E2$ strength at that energy. In photon scattering, this is the case only for that asym-

TABLE V. Three-parameter Fermi parametrization[a] of the charge density of carbon and calcium.[b]

Nucleus	c (fm)	t (fm)	w	$\langle r^2\rangle^{1/2}$ (fm)
C	2.36	0.52	−0.23	2.44
Ca	3.67	0.58	−0.10	3.48

[a] $\rho(r)=\rho_0\{(1+wr^2/c^2)/[1+\exp(r-c)/t]\}$.
[b] Reference 19.

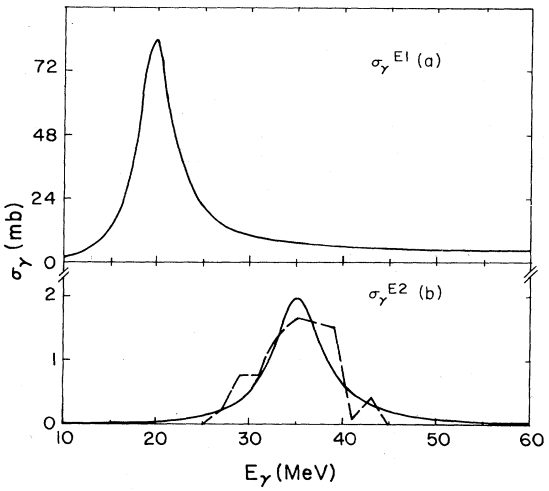

FIG. 4. Result of a computer simulation exercise. Pseudo-data were generated using σ_γ^{E1} shown in (a) and σ_γ^{E2} shown by the solid curve in (b). The $E2$ photoabsorption inferred from the pseudo-data is shown as the dashed curve in (b).

metry due to the imaginary part of the scattering amplitude. The real amplitude gives rise to an asymmetry that depends on the $E2$ strength at all energies, via the DR. As emphasized already, a detailed analysis will be possible only if the scattering measurements span the full energy range of the $E2$ strength.

The feasibility of the procedure for extracting σ_γ^{E1} and σ_γ^{E2} from the scattering data was investigated with computer simulation experiments, in which σ_γ^{E1} [shown in Fig. 4(a)] was specified to be the sum of a giant dipole resonance and a quasi-deuteron tail and σ_γ^{E2} was specified to be a simple Lorentzian. These were then used to generate pseudo-elastic scattering data, with correct statistical fluctuations. The pseudo-data were then used to extract σ_γ^{E1} and σ_γ^{E2}, using the technique described above. Both σ_γ^{E1} and σ_γ^{E2} were defined as piecewise linear functions whose parameters were adjusted to best fit the pseudo-data. The extracted function σ_γ^{E2} is compared with the actual Lorentzian in Fig. 4(b). The agreement is quite good. Furthermore, the extracted σ_γ^{E1} was virtually indistinguishable from the curve in Fig. 4(a), thus demonstrating the feasibility as well as the limitations of this technique. It is important to point out the importance of holding the QD absorption fixed during the fitting procedure. It is not reasonable to expect the scattering data to determine the photoabsorption if that function is completely unconstrained outside the energy region where the scattering is measured. Additional computer simulations confirm this intuition.

B. Analysis of the carbon cross sections

The foregoing technique was used to analyze the elastic scattering cross sections at 135°, 45°, and 90° for carbon. The first step was to use the angle-averaged data in order to determine $\sigma_\gamma^{E1}(E)$. The relevant data are shown in Fig. 5; the 90° data were also used but are not shown due to their sparcity. The $E1$ photoabsorption was parametrized

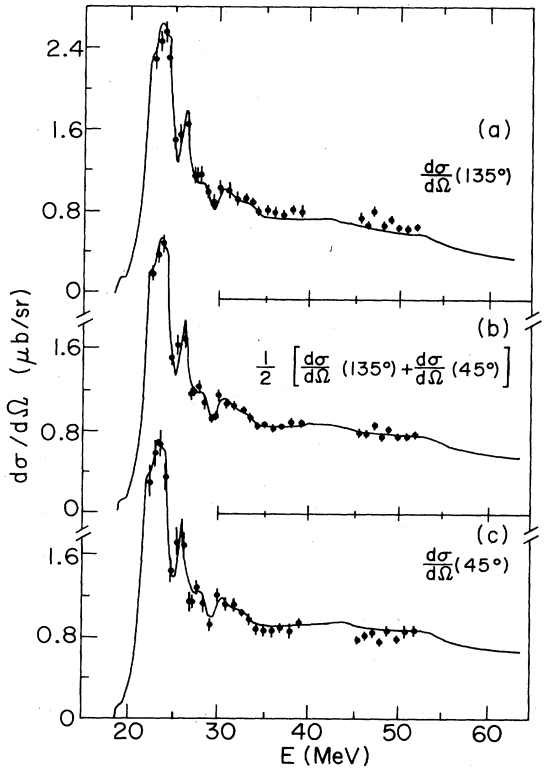

FIG. 5. Elastic scattering cross sections for carbon. The curves are the predicted cross sections based on σ_γ^{E1} inferred from the angle-averaged scattering data (b).

as the sum of a piecewise linear function between 18 and 50 MeV and a quasi-deuteron tail extending to 140 MeV. The latter was fixed independently by fitting to previously measured values of the total photoabsorption cross section $\sigma_\gamma^{\text{expt}}(E)$.[7] Also included were the strong $M1$ line at 15.11 MeV, which exhausts most of the expected $M1$ strength in ^{12}C, as well as $E2$ strength between 22 and 30 MeV that had previously been identified in ^{11}B(p,γ_0)^{12}C.[23]

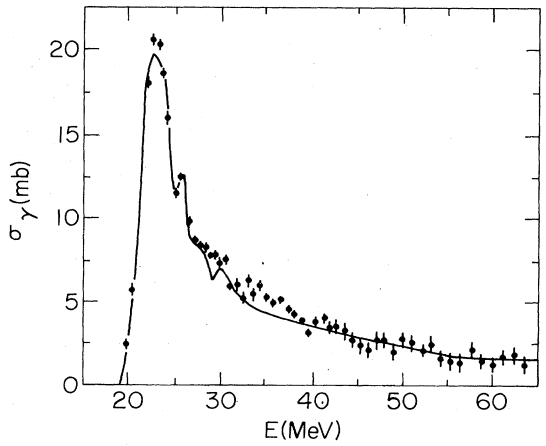

FIG. 6. Photoabsorption cross sections for carbon. The points are the previously reported values for $\sigma_\gamma^{\text{expt}}$ and the curve is the σ_γ^{E1} inferred from the angle-averaged scattering data.

This strength amounts to about 0.2 total (isoscalar plus isovector) energy-weighted sums (TEWS). Finally, since the scattering data extend just barely below the peak of the GDR, it was necessary to include $\sigma_\gamma^{\text{expt}}(E)$ below 26.5 MeV as an additional data set in the fitting. Otherwise it would have been impossible to effectively determine σ_γ^{E1} below about 23 MeV. The fit to the angle-averaged data, shown as the curve in Fig. 5, is excellent.

In Fig. 6 the extracted function $\sigma_\gamma^{E1}(E)$ is compared to the measured *total* photoabsorption cross section $\sigma_\gamma^{\text{expt}}(E)$.[7] These functions agree quite well with each other over the entire energy range shown. In fact, if we compare the integrated cross section up to 50 MeV, they agree to within 6±2%. Furthermore, if σ_γ^{E1} is integrated up to 50 MeV and $\sigma_\gamma^{\text{expt}}$ from 50 to 140 MeV, we find 1.61 classical sums, as compared to 1.67 sums obtained by integrating $\sigma_\gamma^{\text{expt}}$ alone up to 140 MeV. Nevertheless, there is reason to believe that the small discrepancies between 27 and 40 MeV are real, as we discuss below.

Also shown in Fig. 5 are the curves calculated using the extracted σ_γ^{E1} for the scattering cross section at the individual angles of 45° and 135°. The overall good agreement with the data suggests that the $E1$-$E2$ interference effects are small throughout the energy region where we have measured. In particular, the excellent agreement with both the 135° and 45° data below 35 MeV confirms that the scattering in this region is totally dominated by $E1$. On the other hand, above 45 MeV, the curves fall below the 135° data and above the 45° data in just the manner one expects for $E1$-$E2$ interference. This feature is especially clear in the 135° to 45° cross section ratios, shown in Fig. 7. The sign of the interference is what would be expected if the centroid of the $E2$ strength is above 50 MeV. For energies above the centroid, the sign of the interference would change. For example, an improved calculation is shown as the long dashed curve in Fig. 7, which is the result of including roughly 1 TEWS of $E2$ strength in the form of a Lorentzian centered at 55 MeV and with a 12 MeV width. Many other possible distributions of $E2$ strength, all of which are concentrated above 50 MeV, are equally consistent with the data. Although one could attempt to proceed with a second iteration in the fitting procedure in order to extract σ_γ^{E2}, it is clear that since the bulk of the strength lies outside the energy range of the scattering data, these data do not otherwise provide very stringent constraints on the shape of σ_γ^{E2}. Scattering data at higher energy would be needed to extract a detailed shape. However, the fact that there is considerable $E2$ strength above 50 MeV is itself nontrivial, since it is at variance with microscopic random phase approximation (RPA) calculations which predict that most of the $E2$ strength lies below 50 MeV.[24,25] Furthermore, the data do not support any appreciable $E2$ strength ($\gtrsim$0.5 TEWS) between 30 and 45 MeV, as this would require even more $E2$ strength above 50 MeV in order to fit the scattering data. Although this cannot be completely ruled out, it seems unlikely. For example, if one tries to resolve the small discrepancies between σ_γ^{E1} and $\sigma_\gamma^{\text{expt}}$ in the 30—40 MeV range by assuming that their *difference* is due to σ_γ^{E2}, we arrive at the short dashed curve in Fig. 7. This is completely inconsistent with the data. Other distributions of $E2$ strength, e.g., that reported in Ref. 4 or that predicted by the RPA calculations, are equally inconsistent with the scattering data. Other than the NBS result,[4] there are no other reports of $E2$ strength above 30 MeV.

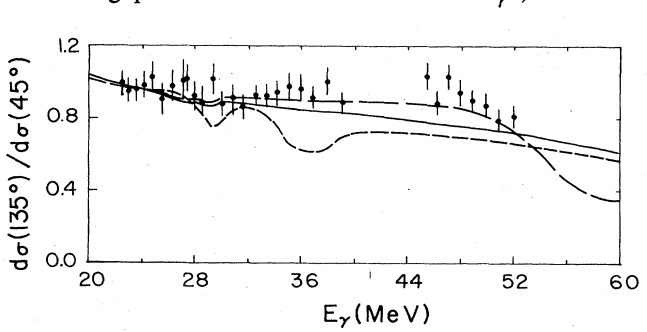

FIG. 7. Ratio of scattering cross sections, $d\sigma(135°)/d\sigma(45°)$, for carbon. The solid curve is calculated from σ_γ^{E1} inferred from the angle-averaged scattering data. The long dashed curve is calculated from this σ_γ^{E1} plus σ_γ^{E2} in the form of a Lorentzian of width 12 MeV, centered at 55 MeV, and exhausting 1 TEWS. The short dashed curve is calculated by assuming $\sigma_\gamma^{E2}=\sigma_\gamma^{\text{expt}}-\sigma_\gamma^{E1}$.

As a side issue, we conclude that there is a small but nevertheless significant discrepancy between the elastic scattering cross section and the total photoabsorption cross section. This discrepancy is not particularly serious in terms of what one might like to know about the total photoabsorption cross section (e.g., sum rules). However, if one would interpret the small discrepancy between $\sigma_\gamma^{\text{expt}}(E)$ and $\sigma_\gamma^{E1}(E)$ as evidence for $E2$ strength, one would greatly overestimate the $E2$ strength in carbon between 30 and 40 MeV. The essential point is that an interpretation of that type is extremely sensitive to the *absolute* cross sections for both $\sigma_\gamma^{\text{expt}}(E)$ and $d\sigma/d\Omega(E,\theta)$. The procedure outlined here, however, does not depend at all on previous measurements of $\sigma_\gamma(E)$ (except to obtain the quasi-deuteron cross section and to constrain the fit below 23 MeV) and, in principle, results in the extraction of $\sigma_\gamma^{E2}(E)$ whose detailed *shape* is quite insensitive to the absolute cross section scale for $d\sigma/d\Omega(E,\theta)$. Unfortunately, as discussed above, it was not possible to obtain a detailed $E2$ strength distribution with the present data.

We now inquire about the extent to which our results depend on the theoretical input. In particular, we examine the consequences of neglecting both the exchange form factor [$F_2(q)=1$] and the nucleon polarizabilities ($\bar{\alpha}=\bar{\beta}=0$) by refitting the scattering data under these conditions. The derived σ_γ^{E1} is slightly smaller than before (about 11% lower between 30 and 50 MeV), but this has only a small (3%) effect on the total integrated cross section (up to 140 MeV). Furthermore, when the calculated scattering cross sections are compared with the data, there is no essential difference with the previous result. Therefore, we are confident that our conclusions for carbon are not very sensitive to uncertainties in the theoretical input.

C. Analysis of the calcium cross sections

The elastic scattering cross sections on calcium were analyzed with the same method used for carbon. First the

angle averaged data were analyzed to determine σ_γ^{E1}, using a parametrization consisting of the sum of a Lorentzian (for the GDR), a piecewise linear function, and a QD tail. The latter was fixed by fitting to the previously measured[7] total photoabsorption cross section $\sigma_\gamma^{\text{expt}}$. Previously reported $E2$ strength below 20 MeV was also included.[26] The results are summarized in Figs. 8–10. The $E1$ strength inferred from the scattering data is compared to $\sigma_\gamma^{\text{expt}}$ in Fig. 9. The discrepancy is much greater than that for carbon. Not only does the GDR appear narrower with σ_γ^{E1}, but also the structure seen in $\sigma_\gamma^{\text{expt}}$ near 40 MeV is absent in σ_γ^{E1} (as well as in the scattering cross sections themselves). As with carbon, the scattering data do not allow these discrepancies to be interpreted as $E2$ strength. However, one should note that the total attenuation method employed by the Mainz group for measuring σ_γ becomes progressively more difficult with increasing Z; calcium is the heaviest nucleus for which this technique has been used.

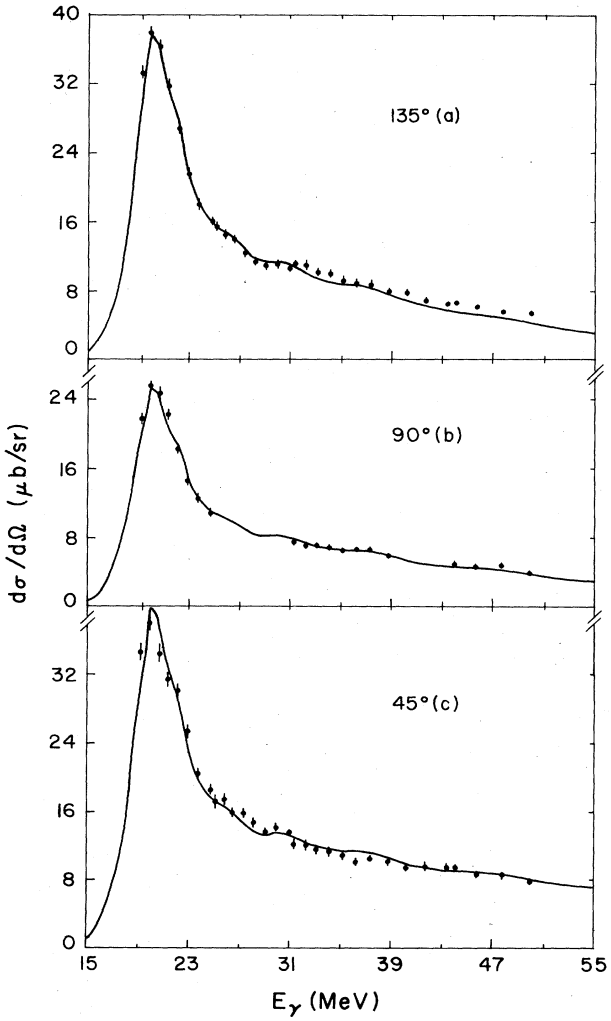

FIG. 8. Elastic scattering cross sections for calcium. The curves are the predicted cross sections based on σ_γ^{E1} inferred from the angle-averaged scattering data.

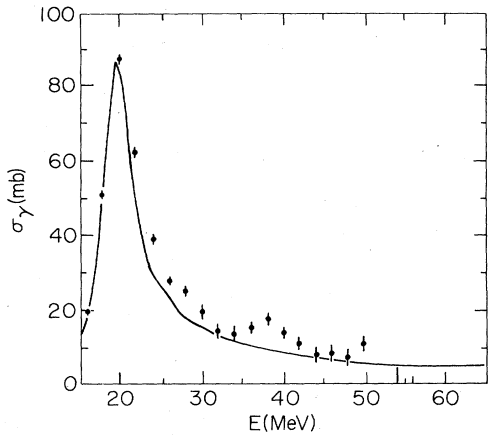

FIG. 9. Photoabsorption cross section for calcium. The points are the previously reported values for $\sigma_\gamma^{\text{expt}}$ and the curve is the σ_γ^{E1} inferred from the angle-averaged scattering data.

The consequences of the smaller photoabsorption derived from the scattering data is explored in Fig. 11, where the world's data on the integrated photoabsorption cross section up to 140 MeV are shown, in units of the classical dipole sum. For $A > 100$, the Saclay data[8] show a nearly constant value of 1.75, whereas the data with $A \leq 40$ show considerable variation with A (Ref. 7). The Mainz value for ^{40}Ca is 2.07, whereas if one uses the values of σ_γ^{E1} derived here below 50 MeV and the Mainz values from 50 to 140 MeV, one obtains 1.80 classical sums, as shown by the open circle. This suggests that already for $A = 40$, the integrated photoabsorption cross section per nucleon has nearly stabilized at a roughly constant value. This result is somewhat more sensitive to the theoretical ingredients than was the case for carbon, presumably because of the larger size of calcium. For example, removing the exchange form factor and the nucleon polarizabilities from the formalism results in an even lower value of 1.70 classical sums.

Although it was possible to obtain an excellent fit to the angle-averaged scattering cross sections, it proved to be

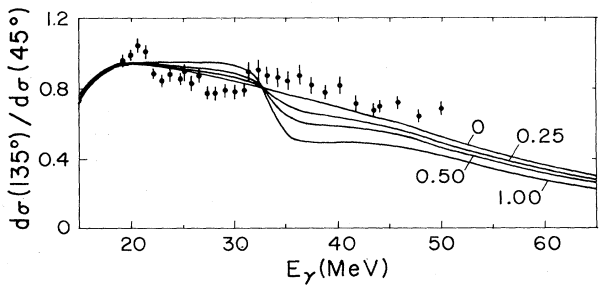

FIG. 10. Ratio of scattering cross sections, $d\sigma(135°)/d\sigma(45°)$, for calcium. The curves are calculated from σ_γ^{E1} inferred from the angle-averaged scattering data plus σ_γ^{E2} in the form of a Lorentzian of width 6 MeV centered at 34 MeV. The numbers indicate how many TEWS are exhausted by the assumed σ_γ^{E2}.

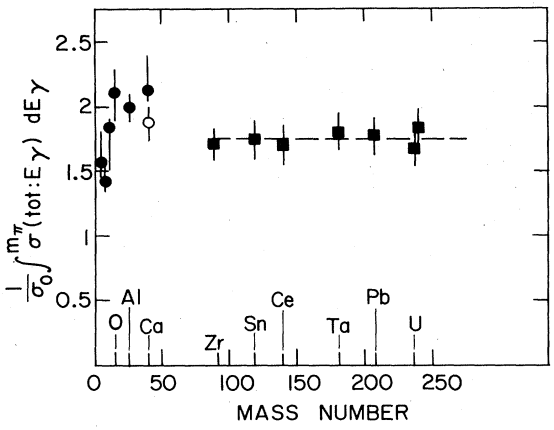

FIG. 11. The world's data for the integral of the total photoabsorption cross section up to 140 MeV, in units of the classical sum. The closed circles are from Ref. 8 and the squares are from Ref. 7. The open circle is the proposed value for calcium deduced from the present data.

impossible to fully understand the cross sections at each individual angle. This is most easily seen in the 135° to 45° cross section ratios (Fig. 10), where the data fluctuate about the curve calculated with σ_γ^{E1} with a phase exactly *opposite* to that expected for $E1$-$E2$ (or $E1$-$M1$) interference. We have no explanation for this behavior; therefore, this represents a fundamental limitation on our ability to extract σ_γ^{E2} from the scattering data. The best that we can do is investigate the overall compatibility of the data with any particular distribution of $E2$ strength. For example, isovector $E2$ strength has been reported in the ^{40}Ca(n,γ)^{41}Ca reaction in the form of a Lorentzian resonance centered around 34 MeV with a width of 6 MeV.[27] In Fig. 10 we show the predicted aft-to-fore ratios when σ_γ^{E1} and various amounts of this $E2$ distribution are used, corresponding to 0, 0.25, 0.5, and 1 TEWS. While none of these curves is really compatible with the data, only the one for 1 TEWS can be ruled out with certainty. The others show structure which is comparable to or less than the unexplained structure in the data, so that they cannot be ruled out. RPA calculations[25] predict about 0.6 TEWS in this energy region.

V. CONCLUSIONS

Elastic photon scattering cross sections were measured at 135°, 90°, and 45° in carbon and in calcium between 19 and 52 MeV. For each nucleus, σ_γ^{E1}, the $E1$ part of the photoabsorption cross section, was deduced from the angle-averaged scattering data using the Mainz photoabsorption measurements, σ_γ, to constrain the cross section at energies where there is no scattering data.

In the case of carbon, the energy integrated values of σ_γ^{E1} and σ_γ are 1.61 and 1.67 classical $E1$ sums, respectively. It was found that the small differences between the inferred σ_γ^{E1} and the measured σ_γ could not be ascribed to $E2$ strength. In fact, the scattering data at 135° and 45° do not admit significant $E2$ strength between 30 and 45 MeV. However, the data do not constrain large amounts of $E2$ strength beyond 50 MeV.

In the case of calcium, the integrals of the inferred σ_γ^{E1} and the measured σ_γ were found to be 1.80 and 2.07 classical $E1$ sums, respectively. The lower value suggests that the $E1$ excess in nuclei may have already saturated at a roughly constant value by $A \approx 40$. The scattering data do not allow the large discrepancies between σ_γ^{E1} and σ_γ to be interpreted as $E2$ strength, although smaller amounts $\lesssim 0.50$ TEWS are not ruled out. Because of unexplained structure in the scattering data, it is not possible to infer stronger conclusions about the distribution of $E2$ strength in calcium.

Recent refinements of the photon scattering formalism were used to analyze the data. Those features that are model dependent have little effect on the conclusions drawn for the $E1$ and $E2$ strength in carbon. However, such modifications may be significant effects upon any conclusions drawn about multipoles higher than $E1$ in calcium.

ACKNOWLEDGMENTS

The authors have benefited greatly from numerous illuminating discussions with Professor S. Fallieros. One of us (A.M.N.) wishes to acknowledge Dr. R. Bergere and Dr. P. Carlos of Saclay for providing a stimulating atmosphere for thinking about the analysis of photon scattering data. This work was supported by the National Science Foundation under Grant No. NSF PHY 83-11717.

*Present address: Department of Physics, Virginia Polytechnic Institute and State University, Blacksburg, VA 24061.

[1]S. S. Hanna, H. F. Glavish, R. Avida, J. R. Calarco, E. Kuhlmann, and R. LaCarma, Phys. Rev. Lett. **32**, 114 (1974).
[2]T. W. Phillips and R. G. Johnson, Phys. Rev. C **20**, 1689 (1979).
[3]D. M. Drake, S. Joly, L. Nilsson, S. A. Wender, K. Aniol, I. Halpern, and D. Storm, Phys. Rev. Lett. **47**, 1581 (1981).
[4]W. R. Dodge, Evans Hayward, R. G. Leicht, Miles McCord, and Richard Starr, Phys. Rev. C **28**, 8 (1983).
[5]R. Leicht, M. Hammen, K. P. Schelhaas, and B. Ziegler, Nucl. Phys. **A362**, 111 (1981).
[6]D. H. Wright, A. M. Nathan, P. T. Debevec, and L. Morford, Phys. Rev. Lett. **52**, 244 (1984).
[7]J. Ahrens, H. Borchert, K. H. Czock, H. B. Eppler, H. Gimm, H. Gundrum, M. Kroning, P. Riehn, G. Sita Ram, A. Zieger, and B. Ziegler, Nucl. Phys. **A251**, 479 (1975).
[8]A. Leprêtre, H. Beil, R. Bergère, P. Carlos, J. Fagot, A. deMiniac, and A. Veyssière, Nucl. Phys. **A367**, 237 (1981).
[9]W. L. Reiter and G. Stengl, Nucl. Instrum. Methods **169**, 469 (1980).
[10]R. G. Sachs and N. Austern, Phys. Rev. **81**, 705 (1951).
[11]J. L. Friar, Ann. Phys. (N.Y.) **95**, 170 (1975).
[12]M. Gell-Mann, M. L. Goldberger, and W. E. Thirring, Phys. Rev. **95**, 1612 (1954).
[13]J. L. Friar and S. Fallieros, Phys. Rev. C **11**, 277 (1975).

[14]J. L. Friar and S. Fallieros, Phys. Rev. C **15**, 365 (1977).
[15]M. Weyrauch and H. Arenhövel, Nucl. Phys. **A408**, 425 (1983).
[16]M. Weyrauch, Ph.D. thesis, Universität Mainz, 1984 (unpublished).
[17]T. E. O. Ericson and J. Hufner, Nucl. Phys. **B57**, 603 (1973).
[18]M. Weyrauch and H. Arenhövel, Phys. Lett. **134B**, 21 (1984).
[19]C. W. deJager, H. deVries, and C. deVries, At. Data. Nucl. Data Tables **14**, 479 (1979).
[20]D. Drechsel and A. Russo, Phys. Lett. **137B**, 294 (1984).
[21]H. Arenhövel, private communication.
[22]M. Weyrauch, diploma thesis, Universität Mainz, 1980 (unpublished).
[23]D. G. Mavis, Ph.D. thesis, Stanford University, 1977 (unpublished); S. S. Hanna, in *Giant Multipole Resonances,* Nuclear Science Research Conference Series, edited by F. E. Bertrand (Harwood, New York, 1979), Vol. I, p. 25.
[24]Giampaola Co and Siegfried Krewald, Phys. Lett. **137B**, 145 (1984).
[25]M. Cavinato, M. Marangoni, P. L. Ottaviani, and A. M. Saruis, Nucl. Phys. **A373**, 445 (1982).
[26]D. H. Youngblood, A. D. Bacher, D. R. Brown, J. D. Bronson, J. M. Moss, and C. M. Rozsa, Phys. Rev. C **15**, 246 (1977).
[27]I. Bergqvist, R. Zorro, A. Hakansson, A. Lindholm, L. Nilsson, N. Olsson, and A. Likar, Nucl. Phys. **A419**, 509 (1984).